# Modeling and Analysis for Nutation Time Constant Determination of On-Axis Diaphragm Tanks on Spinners: Application to the Deep Space One Spacecraft*

Marco B. Quadrelli†

January 7, 2003

## ABSTRACT

This paper describes the modeling, analysis, and testing done to determine the DS1 nutation time constant. The significance of this analysis and testing program is that Deep Space One was the first spacecraft flown by JPL with a diaphragm tank located on the spin axis. First, modeling considerations are made, and in order to simulate the nonlinear behavior of the spacecraft containing the liquid (Hydrazine), the dynamics of a rigid body coupled through a universal joint to a pendulum mass representing the liquid slosh has been analyzed. This nonlinear simulation is done in order to estimate the nutation time constant with a pendulum slosh model. Second, some consideratios follow on the modeling of tanks with diaphragms in spinner tanks. Third, the actual spin drop tests are described. These tests also confirm a nutation time constant in excess of 1000 seconds, both in the case of tests done for the Xenon tank only and in the case of tests done for the Hydrazine tank only. The large value of the nutation time constant computed and verified by testing for this system ensured that it remained well above the required values of 150 seconds at ignition, and 50 seconds at burnout.

## 1 Introduction

The Nutation Time Constant (NTC) estimate is required for launch vehicle stability analysis. It involves any launch with a spinning upper stage for injection, namely STAR motors, and is supplied by the spacecraft customer. The divergence time constant is a significant input to the Nutation Control System analysis. It establishes initial cone angle at third stage ignition, it contributes to the velocity pointing and loss during motor burn, and establishes cone angle at the start of spacecraft separation. The Deep Space One (DS1) spacecraft utilized a monopropellant hydrazine blowdown propulsion system for attitude control and trajectory correction maneuvers. This system incorporates the use of one spherical, 16.5 inch diameter titanium propellant tank. This tank is mounted on the +Z axis of the spacecraft, and incorporates a semi-rigid elastomeric diaphragm for propellant control/management. Because of the configuration of the tank on the spacecraft, because the spacecraft is spinning at 62.8 rpm at thruster ignition, and because of the nature of the diaphragm, it is important to evaluate the influence of this

*Copyright © 2002 by the American Institute of Aeronautics and Astronautics, Inc. The U.S. Government has a royalty-free license to exercise all rights under the copyright claimed herein for Governmental purposes. All other rights are reserved by the copyright owner.

†Mail Stop 198-326, Jet Propulsion Laboratory, California Institute of Technology, Pasadena, CA 91109-8099, marco@grover.jpl.nasa.gov

particular topology on the nutation divergence time constant of the spacecraft when energy dissipation due to liquid motions is possible. This paper describes the challenges of the problem under investigation, discusses several modeling approaches, and presents a slosh pendulum analysis done to support the study of the effect of an elastomeric diaphragm located inside an on-axis spinning tank. It also covers the testing done to support the modeling and analysis. The drop tests for the hydrazine tank and for the xenon tank give separately two different time constants, $\tau_{Xe}$ and $\tau_{Hy}$, which are combined to give the final system's nutation time constant as $\tau = 1/1/\tau_{Xe} + 1/\tau_{Hy}$.

Tthe problem of fluid-structure interaction and its effect on spacecraft stability is of a feedback nature. In fact, the forces and torques acting on the structural system depend on the pressure distribution on the liquid container walls. On the other hand, the current distribution of vorticity in the body of fluid depends on the current distribution of linear and angular velocities to which the base vehicle is subjected. The wobble amplification characteristics depend on the geometric distribution of the liquid with respect to the vehicle's principal axes. The nutation characteristics of the whole system also depend on the dissipation induced by the liquid viscosity, as well as on the presence and damping characteristics of propellant management devices (baffles, membrane diaphragms, or others). Energy dissipation in spinning bodies containing liquids generally depends on: tank shape and geometry (Spherical, Conospherical, Cylindrical, Isotensoid), tank Fill Fraction (FF), Propellant Management Device (PMD) shape & viscoelastic properties (shape, orientation in tank, material constants), PMD orientation in on-centerline (CL) or off-CL tank, tank location with respect to vehicle centerline and center of mass, interaction with moving center of mass (during burn), and vehicle inertial propertie (inertia ratio $\beta$ ).

It is well known that a prolate spinner is unstable, i.e., if the ratio of the spin to transverse moment of inertia is less than one, and the body is spinning about the axis of minimum moment of inertia, an initially small nutation angle $\theta_0$ will increase in a finite time $\Delta t$ to $\theta_f$ according to the approximate law $\theta_f = \theta_0 \cdot \exp(\frac{\Delta t}{\tau})$ where $\tau$ represents the nutation divergence time constant. The NTC can be obtained from initial analytical modeling. It can also be determined from testing, depending on the applicability of such testing methods and facility availability. Comparisons between analysis, test, and flight data from previous programs should be attempted when feasible, as sometimes it is possible to extrapolate from existing data. The case of the Exosat spacecraft (early eighties)[17] which was a spinner with an on-axis diaphragm tank, is significant: analysis showed that adding the diaphragm decreased the divergent nutation time constant by a factor of 6-7 relative to a bare tank. However, the diaphragm configuration was different than in DS1, and more prone to static and dynamic instability. In,[23] the conclusions of[17] concerning the responsibility of inertial wave resonances on the nutation instability of Exosat are questioned based on the fact that there is no correlation between the Exosat test results and the pre-test predictions (also because the predictions did not take into account the increased damping effects due to the presence of a flexible bladder).

Recent studies of the nutation time constant of the Deep Impact spacecraft,[11] with two on-axis Hydrazine tanks of different dimensions, and to be launched in 2003, also conclude that the liquid induced resonances (and perhaps the nutation synchronous mode described below) may also appear during the pre-burn and post-burn phases.

## 2 Spacecraft Mass Properties and other data

The configuration of the DS1 spacecraft is shown in Figure 1. The STAR 37 FM motor and spacecraft are spin stabilized (spin rate=62.8 rpm); the spherical hydrazine tank (radius = 8.25 in = 0.209 m) is located on the spin axis, directly above the xenon tank; the tank contains 27.8 kg of hydrazine (fill factor = 87.5 percent); the hydrazine tank contains a flexible diaphragm as propellant management device (thickness = 0.06 in, more properties below); the required minimum nutation time constants: 150 seconds at ignition, and 50 seconds at burnout. At launch, the fill level of the equivalent clean tank, i.e., a tank of the same radius as the tank in DS1, but without diaphragm, is 87.5 percent. The liquid mass in the tank is 27.8 kg. The mass properties of the

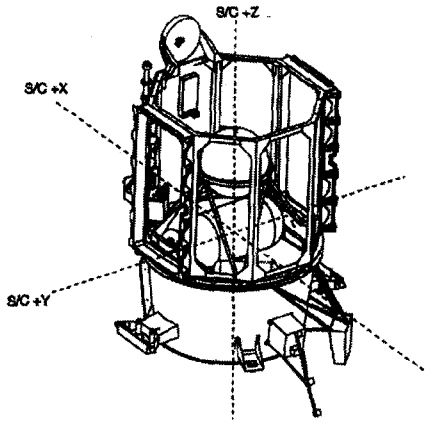


Figure 1: Configuration of the DS1 spacecraft.

whole third stage vehicle (DS1 plus STAR37FM) are as follows:

| | Pre-burn | Pre-Burn | Post-Burn | Post-Burn |
|---|---|---|---|---|
| DS1 s/c cm location (m) | 0.265 | 0.261 | 0.265 | 0.261 |
| mass (slugs) | 117.7 | 117.7 | 44.1 | 44.1 |
| cm location, s/c coords (ft) | -2.87 | -2.91 | -0.425 | -0.522 |
| transverse inertia (slug-ft2) | 925 | 893 | 399 | 388 |
| spin inertia (slug-ft2) | 206 | 206 | 128 | 128 |
| inertia ratio | 0.223 | 0.231 | 0.321 | 0.330 |
| tank center/cm offset (in) | 54.73 | 55.20 | 25.4 | 26.6 |

The liquid fuel parameters of the full scale model are as follows:

| | |
|---|---|
| Tank center location at s/c station | 20.29 inches |
| Tank diameter | 16.5 inches I.D. |
| Fuel | Hydrazine, 87.5 percent fill level |
| Diaphragm Thickness | 0.065 inches |
| Diaphragm Young's modulus | 1200 psi |
| Nominal spin rate | 60 rpm |

# 3 Diaphragm properties and derivation of slosh model parameters

The diaphragm is made of AF-E-332, which is a relatively stiff elastomer. While this material can be stretched to 300 percent of its original length in a uniaxial direction, in its three-dimensional usage the diaphragm can only stretch 10 percent before failing. The diaphragm in this state provides a semi-stiff control surface and is resistant to deformation. Filling of the tank occurs with the diaphragm originally pulled completely toward the propellant side of the tank (i.e., completely evacuated). As the propellant enters the tank, the diaphragm buckles into its reversed position. This buckling can occur in a random direction, and leads to some uncertainties in the

diaphragm ultimate shape. The diaphragm is stiff enough, however, to prevent the fluid from settling into its lowest energy state in the static 1-g environment. The properties of the diaphragm are as follows: tensile strength = 1650 psi, elongation = 260 %, tensile modulus (psi, at 100% elongation)=1200, hardness = 90 points, tear strength = 300 (lb/in), Poisson's ratio = unknown, damping properties = unkown, tensile strength change = -20 %, and elongation change = -20 %.

The last two properties represent the fuel resistance to hydrazine, after 96 hours of exposure at 160 degrees F. In the preliminary evaluation phase of the spin drop test, the scaling of the tensile and bending stiffness of the model diaphragm had to be considered. The spin drop test will be conducted on a 1/3.5 reduced model of the Star37FM motor attached to the casing containing the DS1 vehicle with tank full. The thickness of the diaphragm inside the hydrazine tank needs to be scaled from 1/16th of an inch down to 19/1000th of an inch. The scaled diaphragm needs to be much stiffer than the full scale version, also because a very thin membrane is difficult to manufacture using an injection molding technique. The Young's modulus for the membrane material is 1170 psi for the full scale diaphragm, and 25000 psi for the scaled diaphragm. The bladder is flexible, but nearly inextensible in its reversed position, i.e., at maximum liquid fill level (87.5 percent). The equilibrium shape of the membrane at maximum liquid fill level is axisymmetrical about the +Z axis. This axisymmetry is close to perfect the more the tank is full. The equally important issue of scaling down the diaphragm damping properties remains open, although its effect is unknown and intuitively of less magnitude than that of the stiffness.

From[21] and,[22] the damping ratio can be expressed as a non-dimensional function of diaphragm stiffness and tank diameter for small oscillations. This fact was used in[20] to predict the nutation time constant for Mars Pathfinder. Since DS1 uses exactly the same type of tank as Mars Pathfinder, with the same diaphragm, except that the tank is located on-axis, the extrapolation of the model in[20] to the DS1 model is well justified. As in,[20] we can make the assumption to use data developed for clean tanks (without diaphragm) of diameter $d$ to obtain the fixed pendulum mass $m_f$, the moving (slosh) mass $m_s$, and the pendulum length $l$. We also use the data from[21] obtained for a 20.5 inch diameter tank with 0.010-0.030 inch thick diaphragms to extrapolate and to determine the diaphragm stiffness and damping for the DS1 diaphragm. Since damping increases with increasing diaphragm thickness for spherical tanks ([21]), these estimates of damping are conservative. The pendulum equation of motion in an acceleration field $g = \omega_{spin}^2 d/2$, where d is the tank diameter, is:

$$m_s {l_s}^2 \ddot{\theta} + c\dot{\theta} + k\theta + m_s g l_s sin(\theta) = 0 \tag{1}$$

The pendulum frequency and damping, after linearization, are ${\omega_s}^2 = \frac{g}{l_s} + \frac{k}{m_s {l_s}^2}$ and $\xi = \frac{c}{2\omega_s m_s {l_s}^2}$, respectively. From,[6] the stiffness and damping coefficients for the slosh pendulum can be computed as follows $K_\theta = 0.30 m_s l^2 \omega_{1g}^2$ and $C_\theta = 0.22 m_s l^2 \omega_s$, where $\omega_{1g}$ is the slosh frequency in rad/sec for one-g conditions.

We derive the slosh parameters, i.e., slosh mass, slosh pendulum length, and slosh pendulum hinge point, based on data obtained from Abramson's report[1] for a spherical tank of radius a, with liquid level h (hence fill factor $\frac{h}{2a}$), and fluid density $\rho_f$ with no propellant management devices. An important assumption to keep in mind is that the charts from[1] are derived assuming a horizontal acceleration field, instead of a centrifugal acceleration field. There are no slosh analysis charts reported in the literature assuming as external excitation a uniform rotational acceleration field. Given the 87.5 percent fill factor, the chart in,[1] page 206, provides the following parameters: mass of full tank $m_{full} = \frac{4}{3}\pi\rho_f a^3 = 28.70$kg; effective mass $m_t = \rho_f \pi h^2 (d - \frac{h}{3})$; undamped frequency $\omega_0 = \sqrt{\frac{g}{d}} = 6.8511$rad/sec; $\omega_s = 2.335\omega_0 = 15.997$rad/sec; $m_s = 0.075 m_t = 2.0686$kg; $l_s = 0.335d = 0.07002$m; hinge point location from tank bottom $l_h = 0.99d$; rest mass $m_0 = m_{full} - m_s = 26.631$kg; and rest mass location $l_0 = 0.99d$.

Note that the rest mass is so high because the fill factor is very high, approximating the problem to that of a fully filled spherical tank. Consequently, we assumed the rest mass and the pendulum hinge point to be located at the tank center. The frequency parameter used in Stofan's chart[22] turns out to be $\omega_s \sqrt{\frac{d}{g}} = 2.335$. As a function of diaphragm thickness, linear extrapolation shows the damping ratio to be

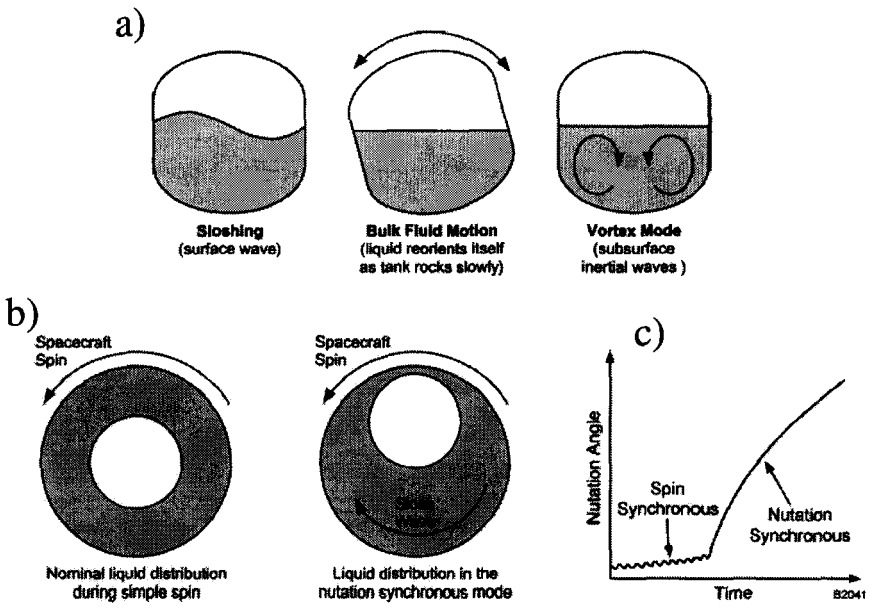


Figure 2: a) Typical modes of fluid motion in tanks. b) spin-synchronous vs. nutation-synchronous mode, c) nutation angle of spin-synchronous vs. nutation-synchronous mode vs. time. (courtesy of Dr. Carl Hubert of Hubert Astronautics Inc.).

| thickness [in] | damping ratio |
|---|---|
| 0.01 | 0.27 |
| 0.02 | 0.38 |
| 0.03 | 0.42 |
| 0.06 | 0.73 |

Consequently, the stiffness and damping coefficients for this configuration become $k = 3.403$N/m and $c = 0.03165$Ns/m, respectively.

# 4 Physics of Liquid-Wall Interaction With and Without Diaphragm

In a fluid-structure interaction problem there are three different modes of fluid motion. See [1], [11] and [8] for a more detailed description of this phenomenon. We refer to Figure 2.

## 4.1 Bulk Motion Mode

In the bulk motion mode (Figure 2a)), the liquid rotates as a rigid body, following the rotational motion of the walls. Bulk fluid motion is characterized by liquid reorienting itself within a tank in response to changes in the tank's alignment relative to the acceleration field and/or inertial space. For example, when a half-filled coffee cup is slowly tilted, the free surface remains horizontal as the liquid repositions itself to minimize its gravitational potential energy. On a spinning vehicle, bulk fluid motion is similar to that of the coffee cup example except

that the shape of the free surface or diaphragm is governed by centrifugal force instead of gravity. Nutation produces a cyclic bulk motion that dissipates energy due to viscous drag as the liquid flows past the tank walls and diaphragm. Unlike free-surface sloshing, bulk motion affects the entire body of the liquid. This means that it can produce much more flow past the tank walls and diaphragm than simple surface wave sloshing. This, in turn, means that under non-resonant conditions bulk motion can dissipate far more energy than sloshing. For a simple spherical tank, bulk motion can be modeled by treating the liquid as a solid body that pivots about the center of the tank. Accurate mechanical analogs are more difficult to develop for non-spherical and diaphragm tanks. Figure 2 c) shows that the nutation synchronous mode is excited in a different manner than the conventional spin synchronous mode. The bulk motion in tanks with internal devices may dissipate a lot more energy than in bare tanks. In fact, the diaphragm causes the fluid-filled spherical cavity to become non-spherical, resulting in a vigorous fluid motion initiated by the viscous boundary layer at the tank walls. In the case of a partially filled cavity, the diaphragm assumes a grossly wrinkled shape which differs from the bare tank free surface. Because the diaphragm causes the fluid-filled cavity to be non-spherical, the liquid motion will dissipate more energy on account of a more turbulent velocity distribution than in a bare tank.

## 4.2 Sloshing Mode

The sloshing mode (Figure 2a)) occurs when the liquid has a free surface, and involves liquid motion in a direction perpendicular to the free surface with very little or no circulation.

The determination of the sloshing oscillations of a fluid in an axisymmetric tank consists of a solution for the velocity potential described by the Laplace equation in three dimensions, which satisfies the prescribed tank wall and boundary conditions and free-surface boundary conditions. From this solution, the equations for the hydrodynamic pressures, forces, moments, surface waveforms, and natural frequencies can be obtained. A simple mechanical analogy in the form of a pendulum or equivalent spring mass will exactly duplicate the forces and moments produced in the fluid oscillations. Physically, the motion of the fluid can be interpreted as follows. A certain portion of the liquid can be considered as rigid and not participating in the sloshing motion, while the fundamental mode reacts as a pendulum and can oscillate as such. The higher modes are not important, as the sloshing masses participating in the motion become smaller as the natural frequency increases. Since the fluid is generally assumed to be incompressible and nonviscous, the mechanical analogy does not apply well in situations where the predominant source of internal recirculation is viscous friction at the tank walls or at the diaphragm surface.

In a spherical diaphragm tank with ullage over the liquid, the diaphragm reduces the wavelength of the slosh mode, increases the frequency, and results in a similar mode shape to the case with the bare tank. The slosh mode frequency and damping ratio increase with diaphragm thickness, and because of the diaphragm viscoelasticity, the free-surface slosh mode is highly damped. The determination of diaphragm viscoelasticity and its effects on this mode are very important.

## 4.3 Nutation Synchronous Mode

The nutation synchronous mode [,[16],[23]] depicted in Figures 2b) and c), involves a unidirectional (non-cyclic) surface wave that revolves around the spin axis at the nutation frequency. On-axis tanks can also support this type of non-oscillatory liquid motion. With an inertia ratio of about 0.2, with a spin rate of 60 rpm, this nutation synchronous wave would circulate around the spin axis at over 40 rpm in a direction opposite to the spin. Such a high velocity flow can dissipate significant amounts of energy and cause rapid nutation growth. A vehicle that experienced this type of behavior is the IMAGE spacecraft, which had no liquid propellant but did have a passive viscous-ring nutation damper that contained 1.2 kg of mercury. The passive damper was for use after separation from the spinning upper stage. The device acted as a de-damper during third stage operations. Pre-flight analysis

indicated that this small amount of mercury could enter the nutation synchronous mode and that if this happened it would require vigorous activity by the NCS. The behavior did occur in flight and Boeing reported that there was more NCS thruster firing during the IMAGE launch than during any other Delta flight.

A good equivalent mechanical model for nutation synchronous motion is a lumped mass traveling on a circular path that is centered on the spin axis. This is essentially the model that was used to predict the performance of the IMAGE damper. Although this model is easy to study by simulation and/or closed form analysis, it is unclear how to select or even bound key model parameters for a spacecraft with an on-axis tank containing a diaphragm. For IMAGE this was simple because the motion involved flow thought a pipe, which is well understood. To excite nutation synchronous behavior requires a minimum nutation amplitude. This critical angle is a function of several parameters, including spin rate, inertia ratio, tank radius, distance from the vehicle cm to the tank center, amount of mobile liquid, and effective damping coefficient. If the effective damping coefficient is low enough and/or the mobile mass is high enough then the critical angle for exciting nutation synchronous motion will be within the range of angles that could be experienced in flight. As indicated by the IMAGE experience, nutation synchronous motion can cause very rapid nutation growth. The difference in nutation growth characteristics under the influence of simple oscillatory spin-synchronous motion and the more vigorous nutation-synchronous motion is shown qualitatively in Figures 2b) and c). Because nutation synchronous behavior is nonlinear, it cannot be analyzed with eigenvalue methods resulting from pendulum models.

## 4.4 Inertial Waves

A rotating fluid supports inertial waves if it is Rayleigh stable [8], i.e. if the angular momentum per unit mass of the circular flow lines increases with the radius from the spin axis. The Rayleigh criterion asks whether the force due to inward radial pressure gradient is adequate to maintain an inward centripetal acceleration for a generic element of the fluid in that rotating flow. If the criterion is satisfied, i.e. if the flow is stable to perturbations, then fluid elements moving radially out or radially inward will tend to return to their initial radius when the perturbation has ceased. Unless the flow is heavily damped (i.e. if baffles are present or the fluid is highly viscous), the element of perturbed fluid will overshoot from the undisturbed radial position, and initiate an oscillatory wave motion called the inertial wave.

Inertial waves (Figure 2a)) correspond to the natural resonant modes for the current tank geometry. They are traveling and also dispersive solutions of a hyperbolic equation [8], which implies that discontinuities can occur in the fluid across characteristic surfaces (cones). These waves die out in a time of the order of the spin-up time (roughly proportional to the square root of the Reynolds number). In a sphere, for example, the first inertial mode is a spin of the interior fluid about a single axis as if it were a rigid body. Higher modes are obtained by seeking smaller subdivisions of the sphere with corresponding motions that satisfy both continuity and momentum balance. Inertial wave modes are a dissipative mechanism which can occur only in spinning tanks, are independent of the presence of a free surface, and can couple with nutational motion. Inertial waves can be excited in non-spherical tanks, and are the result of redistribution of the fluid initiated at the tank walls, progressively diffusing inside the spinning liquid, and these modes have a sectorial character. Inertial waves are driven by the cyclic pressure waves from nutation-induced, angular motions of the tank wall coupled with Coriolis forces inside the liquid. Inertial wave resonances can occur within a bandwidth of two times the spin rate for a prolate spinner, and they can be identified by producing one or more sharp peaks in a plot of the energy dissipated by the liquid in a spinning spacecraft vs. inertia ratio. Because of the sharp energy dissipation that they can produce, the nutation time constant can be drastically reduced if the configuration of the spacecraft is such that the resonance can occur. In a clean fully filled spherical tank, the only fluid-structure interaction mechanism is at the boundary layer at the tank wall, sustained by viscous shear. Inertial waves can occur in fully loaded tanks, with 100% fill factor.

As stated in [24], slosh resonances are generally excited in (forced motion spin table) tests driven at low spin rate (<30 rpm) and high nutation rate (>80 rpm). Conversely, inertial wave resonances, if they exist, should

generally be excited in tests driven at large spin rates (>60 rpm) and small nutation rates (<40 rpm). In their paper, Zedd and Dodge use a rotor model with a viscous damper to model the boundary layer dissipation and the inertial wave resonance.

Unlike the modal decomposition of an elastic member, a spinning fluid does not have a lowest frequency mode and a modal structure in which the frequencies progressively march up from the lowest value to infinity. Rather [15], the eigenvalues tend to cluster in the interval $\{-2\Omega, 2\Omega\}$, where $\Omega$ is the spin rate with numerous excursions outside this interval when a free surface is present. Hence, the fluid modes cannot be ordered according to the magnitude of the eigenvalue. Instead, this ordering is based on the number of nodal surfaces that a particular mode has.

In order to excite these inertial wave modes, energy must be introduced into the flow. For a clean sphere, the excitation may originate at the viscous boundary layer with the tank walls. For a nonspherical surface, the forcing function also includes normal velocities of the boundaries relative to the fluid mass. When there is structural symmetry, solutions may be expressed in terms of Legendre polynomials or Bessel functions, which typically represent axisymmetric expansions. Once excited, the inertial waves move both axially and radially, producing conical shear surfaces which can be visualized in the laboratory using transparent tank walls and tracers in the illuminated liquid. In general, one could say that inertial resonances are extremely sensitive to changes in system geometry.

In a clean spherical tank, the only fluid-structure interaction mechanism is at the boundary layer at the tank wall, sustained by viscous shear.

Assuming that the liquid motion is steady, i.e. all transients have died out, the time $T_{spinup}$ it takes for the liquid to reach the steady state angular momentum imposed by the tank walls can be estimated from the following equation[4] $\frac{H_\infty - H_i}{H_i} = exp(\frac{-\alpha\Omega T}{\sqrt{Re}})$, where $H_i$ and $H_\infty$ are the initial and final angular momentum of the liquid about the spin axis, and $\alpha$ is an empirical constant equal to 0.5. $Re = \omega R^2/\nu$ is the Reynolds number based on the tank radius $R$, the spin rate $\omega$, and the fluid viscosity $\nu$. Using the values for Reynolds number and spin rate computed above, the time T required for the fluid to reach 90 percent of its final angular momentum is 933.44 seconds. This means that a steady liquid rotation (and a better environment for the liquid in terms of less chance of inertial waves to couple with the attitude dynamics) will occur in DS1 after 15.56 minutes from spin-up. Clearly, this analysis does not include the presence of the flexible diaphragm, and assumes that the tank is clean and fully loaded with liquid.

Previous experiments done with water and mercury on a non-spinning tank with 17.5 percent ullage (83.5 percent filled)[19] show that the slosh response was found to be very dependent on the stiffness and deformed shape of the tank positive expulsion diaphragm, for tests done under horizontal excitation. The diaphragm altered the free surface of the fluid by supporting the fluid away from the tank walls. As a result, the classical first free surface slosh mode which is represented by a fluid pendulum motion does not occur. Therefore, the system stiffness appeared to be almost entirely controlled by the stiffness and shape of the diaphragm. In addition, in[19] it was also established that a single multiple degree of freedom pendulum model could not be assumed across the entire frequency range of operation for the tests, rather different models had to be used in different frequency ranges.

A report by F. Dodge on the NEAR spacecraft,[4] which had a spinning tank with a similar on-axis tank configuration with diaphragm, presents some of the issues of interest in the model. Since the tanks are located on the spin axis, spinning simply causes the propellant and diaphragm to be oriented in an axisymmetric shape about the spin axis. No significant lateral shifting of the spacecraft center of mass from the axis was expected. Given the absence of internal hardware, the viscous stresses at the walls are the only available mechanisms to cause the liquids to rotate. There is a very complicated transient liquid flow pattern during spin up, caused by growing boundary layers, internal recirculation flows, and tank end effects.

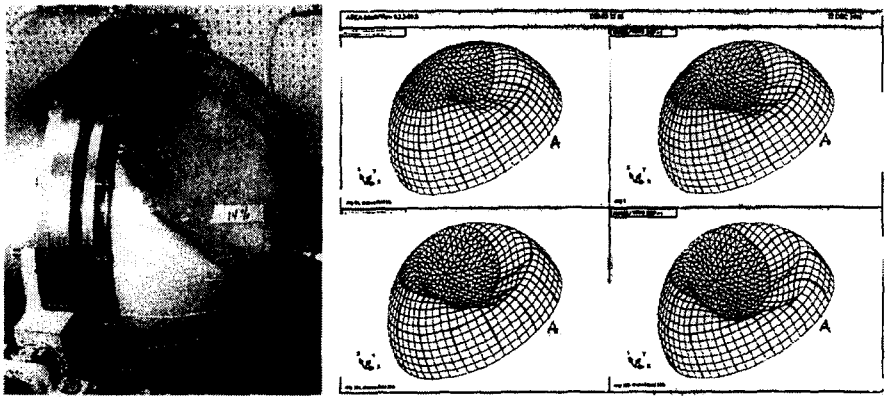

Figure 3: Mars Polar Lander test of tank with diaphragm (right). Modes of deformation of an elastomeric diaphragm inside a draining tank, from[14] (left).

In general, the presence of a diaphragm inside a fuel tank adds a significant uncertainty to the vehicle dynamics of a spinner spacecraft. One remarkable case was EXOSAT (another spinner spacecraft with on-axis tank with diaphragm), in which tests showed that the major sources of dissipation were the internal modes and not the free surface slosh modes, that the effect of the diaphragm orientation inside the tank is crucial for determining the fluid regime, and that adding diaphragms to the propellant tanks decreased the divergent nutation time constant by a factor of 6 or 7 relative to the bare tank. Generally, to ensure success, the configuration to be flown must lie within the parameter space of previously tested or flown configurations, the reason being that there is a significant sensitivity to parameter variations (fill fraction, tank shape, inertia ratio, etc). Figure 3 depicts the grossly deformed diaphragm of a hydrazyne tank used for the Mars Polar Lander spacecraft, and shows some modes of deformation of an elastomeric diaphragm inside a draining tank, obtained from a recent report.[14] The analysis in,[14] although quite detailed and promising, is limited to small deformations of an elastomeric bladder, under gravity, and the fluid contribution is obtained from a pressure equilibrium in a one g field only.

# 5 Pendulum Models

The pendulum model is routinely used by the aerospace industry to provide a solution to the slosh problem to first order of approximation. Unfortunately, it can be useful only to roughly estimate the nutation divergence time constant, and it is not useful for accurate predictions. Traditionally, analytical (pendulum) models often grossly underestimate the severity of the resonances occurring in the fluid-structure interaction process. The presence of a propellant management device (PMD) could be incorporated into the pendulum model via a rotary stiffness and damping coefficient, thereby providing a viscoelastic model of a pendulum as in Figure 4. One the one hand (like the spring-mass-damper oscillator) it provides some back of the envelope estimates. On the other hand, the true physics ends up not being correctly included in the model mainly because it is more of an art to determine the parameters to be used in the model. Pendulum models have indeed been used in the past, and successful examples are in[12] and[13] for the TDRS spacecraft, in[20] for the Mars Pathfinder spacecraft, in,[16] and in,[4],[5] and.[6]

As stated above, the determination of the forced oscillations of a fluid in a tank of axisymmetric shape consists of a solution for the velocity potential described by the Laplace equation in three dimensions, which satisfies the prescribed tank wall and boundary conditions and free-surface boundary conditions. Once this solution, has been obtained, the equations for the hydrodynamic pressures, forces, moments, surface waveforms, and natural

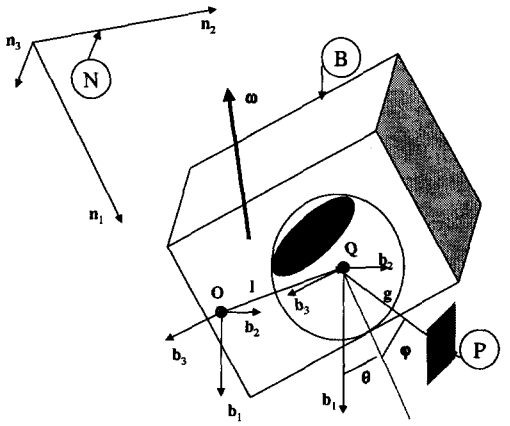


Figure 4: One mechanical model for nonlinear time simulation.

frequencies are combined to compute the effects of the variation in velocity potential. The mechanical analogy in the form of a pendulum or equivalent spring mass will exactly duplicate the forces and moments produced in the fluid oscillations, up to any order in a series expansion of the velocity potential. The physical equivalence consists in having a certain portion of the liquid that can be considered rigid and not participating in the sloshing motion, while the fundamental sloshing mode reacts as a pendulum and can oscillate as such. As in any modal analysis, the higher sloshing modes participate in the motion with increasingly smaller amplitudes as the natural frequency increases. One drawback of the pendulum models for sloshing only is its ineffectiveness in captuiring internal recirculation dynamics since the fluid is generally assumed to be incompressible and nonviscous. Consequently, the mechanical analogy does not apply well in situations where the predominant source of internal recirculation is viscous friction at the tank walls or at the diaphragm surface.

One mechanical model which could be used for cases in which internal recirculation may be important is a conical pendulum held by a spherical joint at the tank center. The angular motion parallel to the spin axis is restrained by a torsional spring and damper representing the viscoelasticity of the diaphragm, whereas the motion about the spin axis could be modeled by the third rotational degree of freedom enabled by the spherical joint, which is restrained only by some form of damper representing the friction of the walls. In this way, the Coriolis coupling which becomes the source of the internal inertial waves is more closely captured. The problem then is to model this damping effect.

# 6 Dynamic Analysis and Nutation Time Constant Prediction

A nonlinear simulation was carried out of the slosh pendulum model mounted on a rigid spacecraft for the purpose of determining the nutation time constant explicitly. Since the nutation time constant is an output of a linearized analysis, it is estimated by means of exponential fitting to the output of the nonlinear program. The nonlinear model represents the problem as a free-floating rigid body connected to a point mass by a universal joint. The system is initially spinning about one axis at 62.3 rpm, and an initial nutation angle is given. The simulation is run for the two cases of pre-ignition and burn-out mass properties, and the trend of nutation angle is observed in time.

We adopt a method based on generalized speeds. As shown in Figure 4, we denote by N the reference (newtonian) frame, by B the base body (spacecraft), by P the slosh mass, by O the spacecraft center of mass, by Q the pendulum hinge point, and by P the slosh mass. The base body reference frame is denoted by the unit

vectors $\mathbf{b_i}$. The pendulum length is $h = l_s$ and the hinge point location with respect to the bus center of mass is $\mathbf{l} = l_i\mathbf{b_i}$ (summed on i). The pendulum angles are $\theta$ and $\phi$, so that the position of the P with respect to Q is

$$^{Q}\mathbf{r}^{P} = (hc\phi c\theta)\mathbf{b_1} + (hc\phi s\theta)\mathbf{b_2} + (hs\phi)\mathbf{b_3} \tag{2}$$

Then, the angular velocity of B in N is $^{N}\boldsymbol{\omega}^{B} = \omega_1\mathbf{b_1} + \omega_2\mathbf{b_2} + \omega_3\mathbf{b_3}$, and the angular velocity of P in N is

$$^{N}\boldsymbol{\omega}^{P} = (\omega_1 + \dot{\phi}sin\theta)\mathbf{b_1} + (\omega_2 - \dot{\phi}cos\theta)\mathbf{b_2} + (\omega_3 + \dot{\theta})\mathbf{b_3} \tag{3}$$

The linear velocity of O in N is $^{N}\mathbf{v}^{O} = u_1\mathbf{b_1} + u_2\mathbf{b_2} + u_3\mathbf{b_3}$. The linear velocity of P in N is

$$\begin{aligned} ^{N}\mathbf{v}^{P} \quad = \quad & [u_1 + \omega_2(l_3 + hs\phi) - h\dot{\phi}s\phi c\theta - \omega_3(l_2 + hc\phi s\theta) - h\dot{\theta}c\phi s\theta]\mathbf{b_1} + \\ & [u_2 + \omega_3(l_1 + hc\phi c\theta) + h\dot{\theta}c\phi c\theta - \omega_1(l_3 + hs\phi) - h\dot{\phi}c\phi s\theta s\phi]\mathbf{b_2} + \\ & [u_3 + \omega_1(l_2 + hc\phi s\theta) - \omega_2(l_1 + hc\phi c\theta) + h\dot{\phi}c\phi]\mathbf{b_3} \end{aligned} \tag{4}$$

With this information, we are ready to extract the partial linear and angular velocities, which we denote by $^{N}\mathbf{v}_r^{O}$, $^{N}\mathbf{v}_r^{Q}$, $^{N}\mathbf{v}_r^{P}$, $^{N}\boldsymbol{\omega}_\mathbf{r}{}^{B}$, and $^{N}\boldsymbol{\omega}_\mathbf{r}{}^{P}$, where $r = 1, ..., 8$, and we have chosen as generalized speeds the quantities $u_1$, $u_2$, $u_3$, $\omega_1$, $\omega_2$, $\omega_3$, $\dot{\theta}$, and $\dot{\phi}$ respectively. We obtain the following list of partial velocities:

| r | $^{N}\boldsymbol{\omega}_\mathbf{r}{}^{B}$ | $^{N}\boldsymbol{\omega}_\mathbf{r}{}^{P}$ | $^{N}\mathbf{v}_r^{O}$ | $^{N}\mathbf{v}_r^{Q}$ | $^{N}\mathbf{v}_r^{P}$ |
|---|---|---|---|---|---|
| 1 | 0 | 0 | $\mathbf{b_1}$ | $\mathbf{b_1}$ | $\mathbf{b_1}$ |
| 2 | 0 | 0 | $\mathbf{b_2}$ | $\mathbf{b_2}$ | $\mathbf{b_2}$ |
| 3 | 0 | 0 | $\mathbf{b_3}$ | $\mathbf{b_3}$ | $\mathbf{b_3}$ |
| 4 | $\mathbf{b_1}$ | $\mathbf{b_1}$ | 0 | $l_2\mathbf{b_3} - l_3\mathbf{b_2}$ | $z_2\mathbf{b_3} - z_3\mathbf{b_2}$ |
| 5 | $\mathbf{b_2}$ | $\mathbf{b_2}$ | 0 | $l_3\mathbf{b_1} - l_1\mathbf{b_3}$ | $z_2\mathbf{b_3} - z_3\mathbf{b_2}$ |
| 6 | $\mathbf{b_3}$ | $\mathbf{b_3}$ | 0 | $l_1\mathbf{b_2} - l_2\mathbf{b_1}$ | $z_2\mathbf{b_3} - z_3\mathbf{b_2}$ |
| 7 | 0 | $\mathbf{b_3}$ | 0 | 0 | $gt_1\mathbf{b_1} + gt_2\mathbf{b_2}$ |
| 8 | 0 | $s\theta\mathbf{b_1} - c\theta\mathbf{b_2}$ | 0 | 0 | $gf_1\mathbf{b_1} + gf_2\mathbf{b_2} + gf_3\mathbf{b_3}$ |

where $z_1 = l_1 + hc\theta c\phi$, $z_2 = l_2 + hs\theta c\phi$, $z_3 = l_3 + hs\phi$, $gt_1 = -hs\theta c\phi$, $gt_2 = +hc\theta c\phi$, $gf_1 = -hc\theta s\phi$, $gf_2 = -hs\theta s\phi$, and $gf_3 = +hc\phi$.

The entries of the inertia matrix may be obtained as follows (k = number of bodies, K = c.o.m. of k-th body):

$$m_{rs} = \sum_{k=1}^{2}(m^{k\,N}\mathbf{v}_r{}^{K} \cdot {}^{N}\mathbf{v}_s{}^{K} + {}^{N}\boldsymbol{\omega}_r{}^{K} \cdot \mathbf{I}^{K} \cdot {}^{N}\boldsymbol{\omega}_s{}^{K}) \tag{5}$$

where $\mathbf{I}^2 = \mathbf{0}$ since it is only a mass point.

The equations of motion in the generalized speeds may be written as $M\dot{\mathbf{u}} = \tau$, where

$$\tau_r = -\sum_{k=1}^{2}({}^{N}\mathbf{v}_r{}^{K} \cdot F_t{}^{k} + {}^{N}\boldsymbol{\omega}_r{}^{K} \cdot T_t{}^{k}) \tag{6}$$

and

$$F_t{}^{k} = m^k\mathbf{a}_t^k - F_e{}^{k} \tag{7}$$

$$T_t{}^{k} = \mathbf{I}^k\boldsymbol{\alpha}_t^k + \boldsymbol{\omega}^k \times \mathbf{I}^k\boldsymbol{\omega}^k - T_e{}^{k} \tag{8}$$

Here, $\mathbf{a}_t^k$ and $\boldsymbol{\alpha}_t^k$ denote the linear and angular acceleration remainder terms (second total accelerations minus contribution to inertia matrix), and $F_e{}^{k}$ and $T_e{}^{k}$ denote the external forces and torques. The external forces are zero, as well as the external torque on the base body. The external torque on the pendulum is given by

$$T_e{}^{2} = n_\phi s\theta\mathbf{b_1} - n_\phi c\theta\mathbf{b_2} + n_\theta\mathbf{b_3} \tag{9}$$

where $n_\theta = -k\theta - c\dot{\theta}$ and $n_\phi = -k\phi - c\dot{\phi}$ are the hinge torques representing the viscoleastic effect of the diaphragm. The rotation of the base body is parameterized by the unit Euler parameters $\mathbf{q} = [e_0 \mathbf{e}]$, so that ${}^N\boldsymbol{\omega}^B = 2G\dot{\mathbf{p}}$ where $G = [-\mathbf{e} - \mathbf{e} \times \mathbf{1} + e_0 \mathbf{1}]$.

The system is simulated for 100 seconds starting from an initial nutation angle of 0.1 degrees. The results show that, for both the pre-ignition and the burn-out cases, a good exponential fit of the divergent nutation angle $\vartheta$ in degrees is provided by the following equations:

$$\vartheta_{ignition} = 0.0996 \exp(t/1590) \tag{10}$$

and by

$$\vartheta_{burnout} = 0.0996 \exp(t/1990) \tag{11}$$

The two nutation time constants are 1590 seconds for pre-ignition, and 1990 seconds for burnout, for the given parameters of the spacecraft and hydrazine slosh model. Figure 5, Figure 6, Figure 7, Figure 8, and Figure 9 depict, respectively, the nutation angle at ignition and burnout vs. time showing the sensitivity to different parameters (center of mass location, diaphragm stiffness and damping), and the phase plane for the angles $\theta$ and $\phi$ vs. time. It is interesting to note that these numbers are significantly different than those that the energy sink analysis predicted without including the effect of the diaphragm. Therefore, we conclude that the results of the slosh pendulum model show no danger of instability. Because the nonlinear slosh dynamic model is more detailed than the energy sink analysis, it is also more realistic. The results shown in Figure 5 assumed a perfectly balanced spacecraft, and the center of mass location (in spacecraft coordinates) was at 10.13 inches along the Z axis (no X or Y components present). However, subsequent mass properties changes resulted in a slight center of mass offset. The new center of mass location is at 10.59 inches along the Z axis, -0.16 inches along the X axis, and -0.37 inches along the Y axis . Some simulations have been run incorporating this new change in the pre-burn and burnout cases, and the results are shown in Figure 6 and Figure 7. The new (computed) nutation time constant is about 900 seconds (pre-burn) and 1450 seconds (burnout). What we can infer from these figures is that the presence of an offset of the center of mass along the X and Y axes starts a wobbling motion of amplitude less that 1 degree, superimposed on the nutational instability typical of a prolate spacecraft. The wobbling remains superimposed, since it is not damped, being equivalent to spinning about a different geometrical axis. Eventually, but only over a long time, is the nutation growth visible in the plot of nutation angle vs. time. Note that in the previous case, i.e. when the center of mass is on the Z axis, the wobble angle is exactly zero, and the attitude motion is governed by the nutational instability, induced by the slosh motion, alone. In the new case, the estimated wobble angle is 0.30 degrees in the pre-burn case, and 0.24 in the burnout case. We see that, besides the wobble angle induced by the center of mass offset, there is an additional contribution to the amplitude of the nutation angle which is due to the wobble amplification induced by the motion of the slosh mass: its effect is similar to having one flexible mode. If in addition, we assume that the spacecraft has been balanced, but imperfectly, so that a residual offset is left along the X and Y axes (in this case, an offset of 3.2e-2 inches along the X and of -3.2e-2 inches along the Y axes), the result is still different, implying that a very slight offset has also the potential of initiating a wobbling motion. In this case, this wobbling motion is of much smaller amplitude. The nutation time constants are practically the same as in the prefectly balanced case, but with some slight wobbling superimposed (1500 seconds for preburn, 1900 seconds for burnout ). The estimated wobble angle is 0.035 degrees for the pre-burn case, and 0.028 for the burnout case. In this case, the wobble amplification due to slosh motion is much less than in the previous case. Figure 9 depicts the nutation angle vs. time at ignition for the cases in which the stiffness and damping coefficients are equal to 10 times larger, and 10 times smaller, respectively, than the reference values given above. From these plots, we see that although the magnitude remains confined to approximately the same value and that the behavior is qualitatively different, an exponential fit would provide in all three cases a very large value of nutation time constant (at least 1000 seconds). At this point we deem necessary to quote[7]: *Using an equivalent dynamic pendulum model...is is impossible to achieve such a simplified equivalence for rotating tanks where Coriolis accelerations and vorticity prevail. Therefore, a pendulum model can only give an incomplete fluid behavior representation.*

The next table summarizes the results:

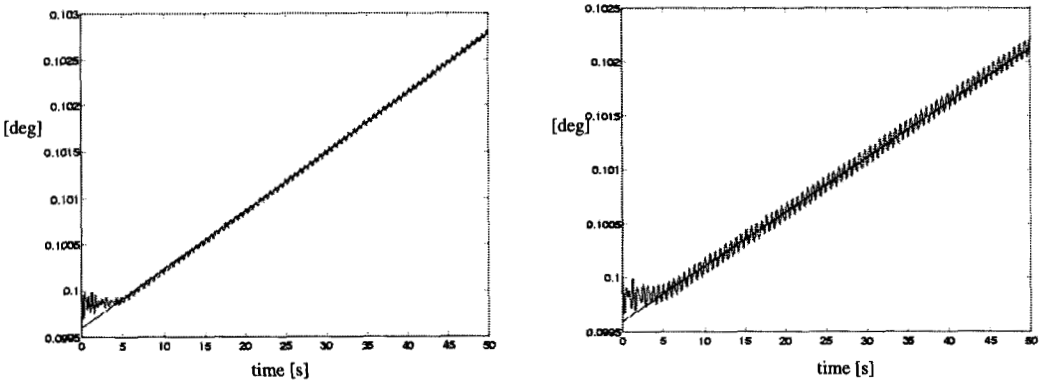


Figure 5: Nutation angle [deg] at ignition (left) and burnout (right) vs. time. com=[0;0;10.13] in

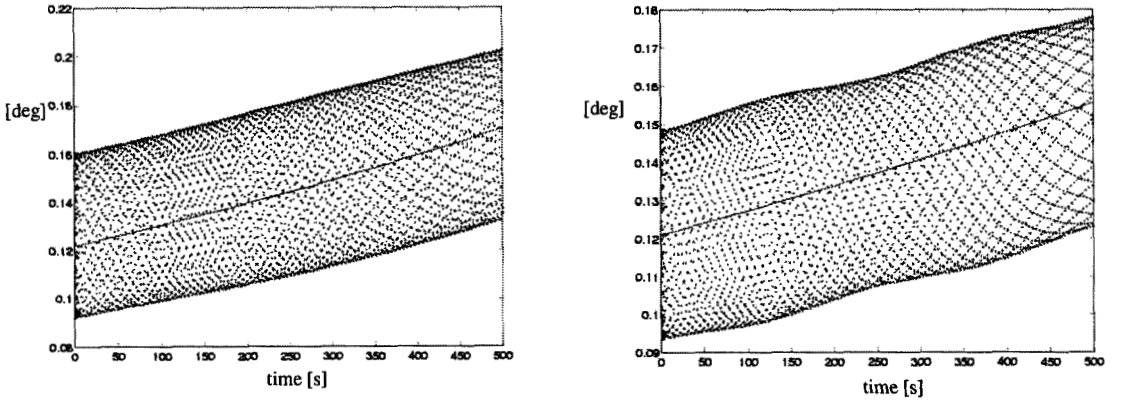


Figure 6: com=[3.2e-2;-3.2e-2;10.59] in

| configuration | wobble angle [deg] | time constant [s] |
|---|---|---|
| preburn (no offset) | 0 | 1590 |
| burnout (no offset) | 0 | 1990 |
| preburn (-0.16,-0.37,10.59) | 0.30 | 900 |
| burnout (-0.16,-0.37,10.59) | 0.24 | 1450 |
| preburn (+0.03,-0.03,10.59) | 0.035 | 1560 |
| burnout (+0.03,-0.03,10.59) | 0.028 | 1960 |

In conclusion, the effect of having a center of mass off the Z axis is to reduce the time constant (even a slight offset causes this reduction, showing how sensitive the spacecraft is to imbalance), and to induce a wobbling motion of max amplitude of 0.6 degrees in the preburn case, and a max. amplitude of 0.4 degrees in the burnout case. The wobbling motion is also amplified to some degree by the inertial loading imposed by the moving slosh mass which, from a dynamical point of view, is equivalent to having an additional flexible mode in the system. Nevertheless, these nutation time constants are still well above the minimum requirements, and the wobbling motion is of very small amplitude.

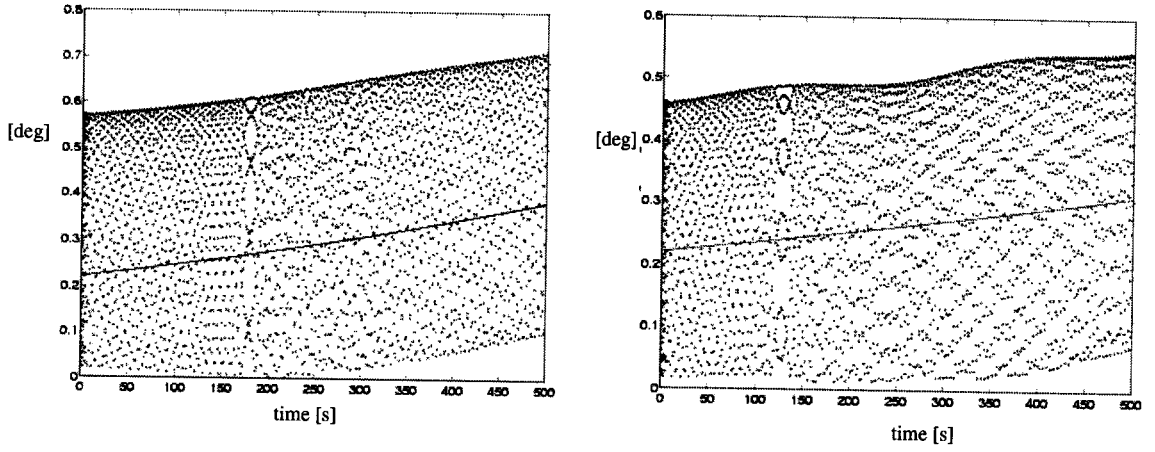


Figure 7: com=[-0.16;-0.37;10.59] in

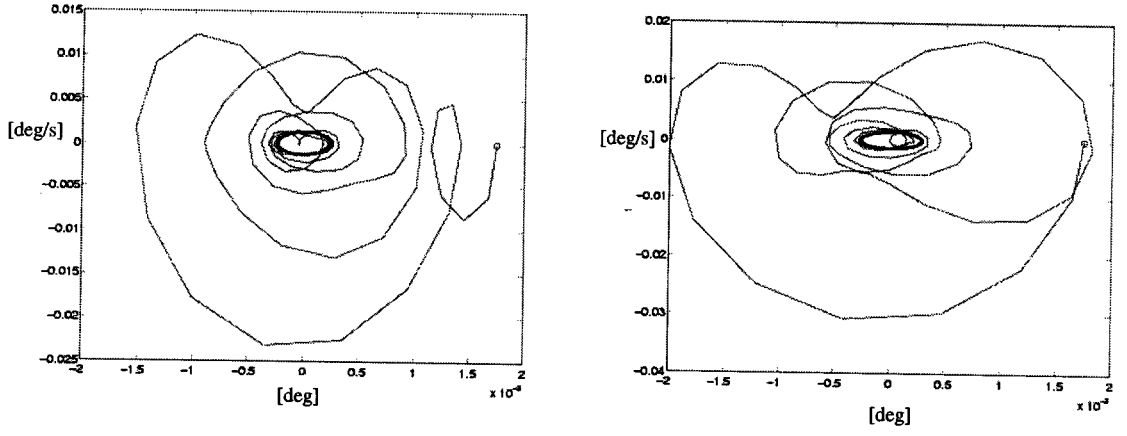


Figure 8: com=[0;0;10.13] in

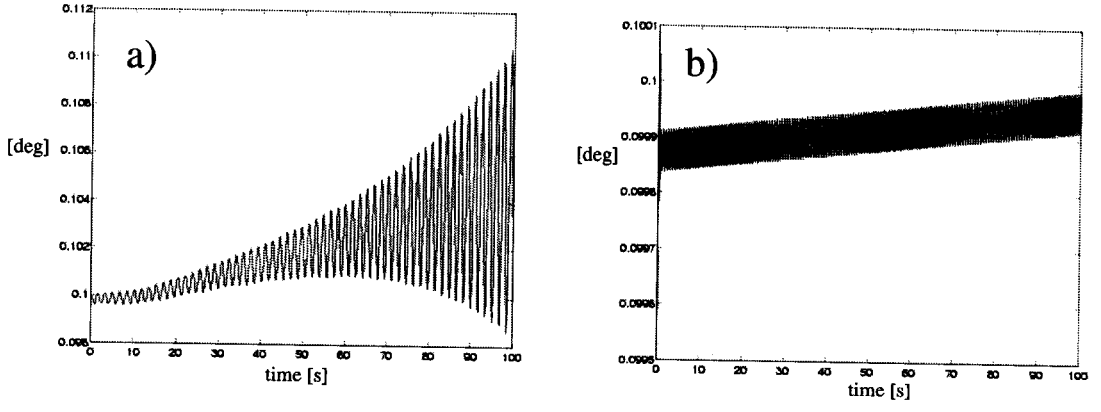


Figure 9: Nutation angle with diaphragm k and c 10 times larger (a) than the reference value described in the text, and with diaphragm k and c 10 times smaller (b).

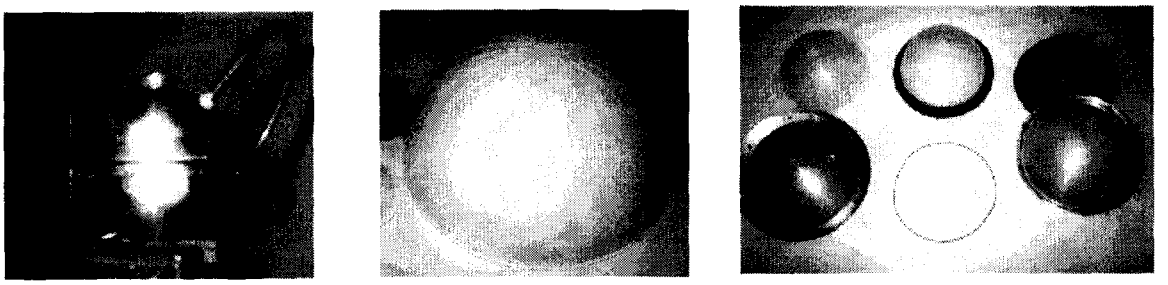

Figure 10: Photograph showing the Deep Space 1 scaled tank being filled with water before the spin drop test, the scaled diaphragm to be placed inside the scaled tank, and the components of the Deep Space 1 model tank with diaphragm.

# 7 Drop Tests

The drop tests were conducted by Dr. Jon Harrison at the ADL (Applied Dynamics Laboratories, Roseburg, OR) drop tower test facility. The facility is located in a three story building especially designed for all aspects of drop test model research, design, construction, testing, and data reduction and analysis. The basement area is used for storage of model construction materials, the first floor is used as a machine shop, and the second floor is the office, data reduction, and computer area. The drop tower is located at one end of the building. The hardware specifically related to drop testing includes the following: spinup/release mechanism; tower and catch box; telemetry and data processing system. Figure 10 shows details of one scaled tank with the internal structure of the scaled rubber diaphragm used in some of the drop tests.

# 8 Phase I: DS1 Xenon Tank Drop Test Program

The drop tests for the xenon tank use a drop test model with a 1/5 scale model of the xenon tank filled with an appropriately scaled liquid. The nominal spin rate of the full scale vehicle is 60 rpm, and the nominal inertia ratios are 0.222 (pre-burn) and 0.296 (post-burn). Along with predicting the nutation time constant for the nominal parameters, the main effort of the test program is to uncover any fluid resonances that may exist. The search was limited to inertia ratios approximately 10% above and below the nominal values with an increment of approximately 0.01. Ballast weights on the model are adjusted to change the inertia ratio. The time constant for the full-scale vehicle is computed by scaling the model results using scaling laws based on the Energy Sink assumptions.

The spacecraft/upper stage mass properties used in the determination of the xenon tank time constant are as follows:

| | pre-burn | post-burn |
|---|---|---|
| Spin inertia (slug-ft2) | 200 | 121 |
| Transverse inertia (slug-ft2) | 897 | 409 |
| Inertia Ratio | 0.222 | 0.296 |

The interior of the xenon tank is a 19.3 inch long cylinder with identically domed ends. The volume is 50 liters. The tank load is between 63 and 83 kg. Since the tank volume is 50 liters, the fluid density is approximately

1.2 and 1.7 kg/liter. The full scale test results are based on the higher density since that gives the shortest time constant. The kinematic viscosity for any load is approximately 0.054 centistokes.

The design of the model is driven by the need to accurately simulate the xenon fluid. The two scaling laws that are relevant are the Mach number ($d\omega/V$) and Reynolds number ($d^2\omega/\nu$), where d=tank diameter, $\omega$ is the spin rate, V is the velocity of sound in fluid, and $\nu$ is the kinematic viscosity. The full scale Mach number is between 0.0055 and 0.0124. This is so much less than one that compressibility effects are of much less importance than viscosity effects. Therefore, the model, which uses a liquid to represent the xenon, is designed to accurately match Reynolds number.

The xenon fluid has a very low viscosity which in turn requires a very low viscosity model liquid. The liquid used is a 1,1,2 Trichloroethane. It has a density of 1.44 kg/liter and a kinematic viscosity of 0.083 centistokes (1/12 that of water). With a length scale of 1/5, the Reynolds numbers exactly match at a model spin rate of 2300 rpm. This is used for all tests.

No data were found for the velocity of sound in 1,1,2 Trichloroethane but, based on data for other similar liquids, it is estimated that the value is approximately 1500 meters/second. The Mach number for the model is, therefore, approximately 0.01 which is close to the full scale value. Since the Mach numbers for the model and the full scale vehicle are 1) so much less than one, and 2) so closely match, it is felt that the model liquid accurately simulates the xenon fluid, a compressed gas.

The model tank is constructed in two halves which are sealed with an O-ring and bolted together. The tank is an exact 1/5 scale replica of the full scale tank. The cylinder and domed ends are machined on a computer controlled lathe with the R-S coordinate points connected by a smooth curve. The main body of the drop test model is a 6 inch diameter, 12 inch long PVC tube with aluminum end caps. The tank is mounted to the tube with screws through each end of the tank. One of these screws serves as a fill/drain port. Lead weights are added around the circumference of the tube to achieve the desired inertia ratio.

The scaling law $\rho d^5 \omega \tau / J = constant$ is based on the Energy Sink assumptions and is used to scale the data for the model and full scale vehicle, where d=tank diameter, $\omega$ is the spin rate, $\rho$ is the liquid density, $\tau$ is the nutation time constant, J is the spin moment of inertia. Using the full scale values for moment of inertia, the scaling laws become $\tau_{FS} = 9628\tau_M/J_M$ in the pre-burn case, and $\tau_{FS} = 5825\tau_M/J_M$ in the post-burn case, where the subscript M refers to the model, and FS to the full scale vehicle. The model spin inertia $J_M$ changes somewhat as ballast is added or removed to alter the inertia ratio.

## 8.1 Test Results

The results from the tests are summarized in Figure 11. The data can be corrected for the effects of air damping and parasitic energy dissipation by using an appropriate tare value. The nutation angles at the beginning and at the end of the drop are shown as well of the inertia ratio (as determined by the spin speed and nutation frequency) and the model time constant. The latter is computed by finding the exponential curve which best fits the data. Tests DS3, 4, and 12 are tare tests. These test are run without liquid, with rigid ballast replacing the tank and liquid, to determine the effect of air drag and parasitic structural energy dissipation. The results show extremely long time constants which means these effects are negligible. In the rest of the tests, the tank is completely filled with liquid. In one test (DS22), a liquid with a viscosity 7.7 times higher than the regular test liquid (but the same density) is used. This was done to see the effect of the Reynolds number error. Comparison of the results of this test and DS11 (with the lower viscosity) shows a significant difference. Tests DS10 and DS11 differ only in initial nutation angle. The results show no sensitivity to nutation angle. Tests DS3 to DS11 are considered to be pre-burn cases since they range in inertia ratio from 13 % below to 9% above the nominal value (0.222). Similarly, tests DS12 to DS 21 are the post-burn cases since they range in inertia ratios from 15% below to 9% above the nominal value (0.296).

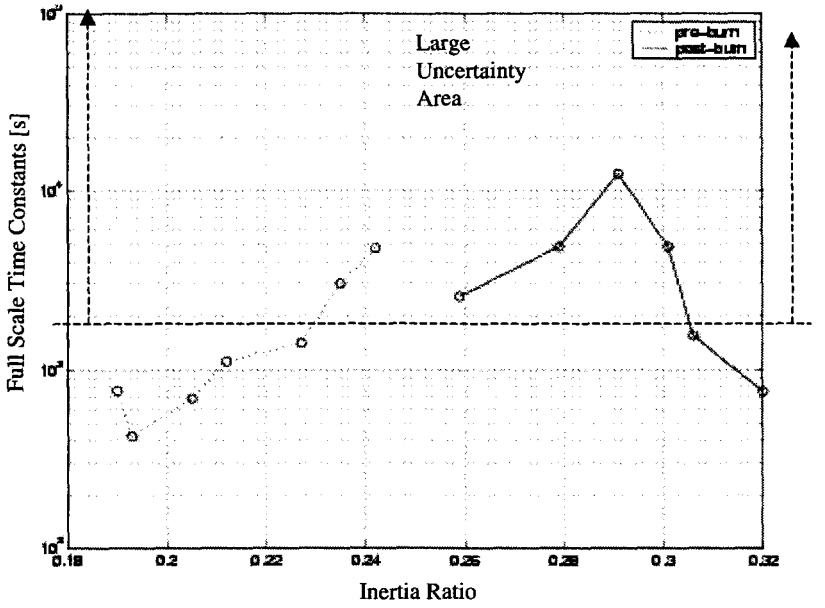


Figure 11: Full scale time constants in the pre- and post-burn cases vs. inertia ratio for the Xenon tank.

The tests results indicate full scale pre-burn time constants in excess of 1000 seconds for all inertia ratios above 0.21. Below 0.21 inertia ratio, the data indicate that a liquid resonance mode exists at approximately 0.19 inertia ratio. The pre-burn and post-burn results are plotted in Figure 11. Note that there is significant uncertainty in the data for model time constants above about five seconds (area enclosed within dotted lines). This is the reason for the scatter in the long time constant pre-burn data, as well in the post-burn data. Even though all of the post-burn time constants are long, the data suggests that another resonance mode may exist above inertia ratio 0.33. In conclusion, the nutation time constant considering the presence of the Xenon tank only is in excess of 1000 seconds, which means that the Xenon gas behaves almost like a solid lump, rigidly connected to the tank walls.

# 9 Phase IIa: DS1 Hydrazine Tank Drop Test Program

## 9.1 Introduction

Phase IIa of the hydrazyne tank drop test program was completed with all of the original objectives met. Analytical scaling laws were developed which define the parameters of the model diaphragm. Based on the assumptions and depth of the analysis, a high confidence exists that the model diaphragm was accurately simulating its full-scale counterpart. Three different elastomeric compounds were developed and several diaphragms were made from each type of material. Depending on the material used, the correctly scaled model spin rate is between 870 and 1300 rpm. The diaphragm was successfully installed in the tank, moved into the reversed position, and the tank filled. Many drop tests were performed without any case of leakage or diaphragm breakage. Even though the model did not represent DS1 in terms of mass center location or inertia ratios, it is worthwhile commenting on the nutation behavior. With the tank fill fraction approximately 85 percent, the diaphragm appeared to be slightly stretched and quite rigid. The measured time constants were extremely long. Some tests were run at lower

fill levels, and these resulted in shorter time constants. Presumably, this was due to wrinkles or flexing in the diaphragm when it was not stretched. It should be emphasized that the model tested had the mass center relatively close to the tank center. For DS1, particularly in the pre-burn state, the mass center to tank center distance is quite large. There was a strong possibility that this lever arm would powerfully drive the liquid/diaphragm system and cause short nutation time constants even at high fill levels. The remainder of this section will discuss the scaling laws and model diaphragm in more detail.

## 9.2 Scaling Laws

A detailed analytical study of the equations governing the flexible diaphragm deflection due to the spinning liquid was performed. This analysis resulted in the following diaphragm scaling laws which are dimensionless ratios which must be preserved for both the model and the full-scale vehicle: $h/R$, defines the model diaphragm thickness; $E/\rho R^2\omega^2$, defines the relationship between model spin rate and diaphragm modulus of elasticity, where h is the diaphragm thichness, R is the tank radius, E is the modulus of elasticity of the diaphragm material, $\rho$ is the liquid density, and $\omega$ is the spin speed. It was assumed that the Poisson's ratio is reasonably well matched if the model and the full-scale diaphragm materials are similar. The full-scale parameters are as follows: R=8.25 inches, h=0.065 inches, $\rho$=0.0364 lb/in3, $\omega$=60 rpm, E=1200 lb/in2. The values for E (full-scale and model) are obtained by measuring the deflection (d) of a sample of material (thickness h, width b). The sample is suspended on two knife edge supports (separation l), and a force (W) is applied. The modulus of elasticity is calculated as: $E = Wl^3/4dbh^3$. A model tank of radius 2.375 inches is used with water (.0361 lb/in3) simulating the fuel. The model parameters based on the scaling laws are therefore: h=0.187 inches, $\omega/E$=36.5 ($\omega$ in rp, E in lb/in2).

### 9.2.1 Scaling of fuel-membrane-gas system in a rotating tank

This analysis was done by Prof. Charles Smith, retired from Oregon State University, and describes in some more detail the steps that have led to the numbers indicated above. The analysis was done to identify the way to correctly scale the elastic properties of the diaphragm, i.e. axial and bending stiffness, and see if the Poisson ratio needs to be scaled as well. The analysis considered a spinning rigid tank, an incompressible inviscid fluid in the tank, and an elastic membrane modelled as a shell. Since the output of this analysis would have identified the correct stiffness of the scaled membrane, before manufacturing, and there was uncertainty on the manufacturing process, the possibility existed of having to deal with a composite shell, made of two layers. The quantities involved in this scaling procedure are: $\omega_0$ the initial angular speed of the tank, E the shell elastic modulus, h the shell wall thickness, R the tank radius, I the central inertia dyadic for the rigid portion of the vehicle, $\rho$ the fuel density, p the fuel pressure, $E_1$ ($E_2$) the modulus of the inner (outer) layer of the composite shell, $h_1$ ($h_2$) thickness of inner (outer) layers of composite shell. Then, the tensile stiffness becomes $E_F h_F = E_1 h_1 + E_2 h_2$, and the bending stiffness becomes $E_M h_M^3 = E_2 h_2[h_2^2 + 3h_1(h_1 + h_2)] + E_1 h_1^3$. Introducing the ratios $\alpha = \frac{R_{test}}{R_{fullscale}}$, $\beta = \frac{(\omega_0)_{test}}{(\omega_0)_{fullscale}}$, $\gamma = \frac{\rho_{testliquid}}{\rho_{fuel}}$, the ratios (or nondimensional numbers) that must remain unchanged for the governing equations to remain unchanged are $\frac{I}{\rho R^5}$ to satisfy the momentum equilibrium of the rigid body plus the tank and fluid, $\frac{p}{\rho R^2 \omega_0^2}$ to satisfy the Euler equation for the incompressible, inviscid fluid in the tank, $\frac{pR}{E_F h_F}$ to satisfy the radial equilibrium of a shell element, $\frac{E_M h_M^3}{R^2 E_F h_F}$ to satisfy the moment equilibrium of a shell element. The last two also reduce to the following ones (after recombination with the first two): $\frac{E_f h_F}{\rho R^3 \omega_0^3}$ and $\frac{E_M h_M^3}{\rho R^5 \omega_0^2}$.

With these definitions, the tank diameter D in the test model becomes $D_T = \alpha D$, the spin rate $\omega_0$ in the test model becomes $\omega_{0T} = \beta\omega_0$, the fuel density $\rho$ in the test model becomes $\rho_T = \gamma\rho$, the rigid inertia dyadic I in the test model becomes $I_T = \alpha^5\gamma I$, the membrane tensile stiffness Eh in the test model becomes $E_F h_F = \alpha^3\beta^2\gamma Eh$, and the bending stiffness $Eh^3$ in the test model becomes $E_M h_M^3 = \alpha^5\beta^2\gamma Eh^3$. Given the full scale values of $E = 1200psi$, $\nu = 0.49$, $h = 0.065''$, $D = 16.5''$, $\omega_0 = 60rpm$, $\rho = 0.0361lbm/in^3$, the scaling can be done

following three approaches:

- increase the Young's modulus, so that both the tensile and bending stiffnesses scale properly. In this case, if $D_{test}$=4.75 inches, $\omega_{0T}$=750 rpm, $\alpha = 4.75/16.5$, $\beta = 750/60$, $h_T = 0.0187$ inches, $E_T = 15540$ psi, and if $D_{test}$=3.6 inches, $\omega_{0T}$=750 rpm, $\alpha = 3.6/16.5$, $\beta = 750/60$, $h_T = 0.0142$ inches, $E_T = 8926$ psi.
- Consider a composite shell, for which one obtains: $D_{test}$=4.75 inches, $\omega_{0T}$=58 rpm, $h_1 = 0.013$ inches, $E_1 = 12000$ psi, $h_2 = 0.019$ inches, $E_2 = 1200$ psi.
- Consider the shell material to be the same as in the full-scale tank, scale the thickness so that the bending stiffness is properly scaled, and accept the improperly scaled tensile stiffness. Then, with $D_{test}$=4.75 inches, $\omega_{0T}$=750 rpm, $E = 1200$ psi, $h_T = 0.044$ inches, $Eh_T = 52.8$ lbf/in, and $\alpha^3\beta^2 Eh = 291$ lbf/in, while with with $D_{test}$=3.6 inches, $\omega_{0T}$=750 rpm, $E = 1200$ psi, $h_T = 0.0277$ inches, $Eh_T = 33.2$ lbf/in, and $\alpha^3\beta^2 Eh = 126.6$ lbf/in.

The strain components in the plane tangent to the middle surface of the shell have the form $\epsilon_{ij} = A_{ij} + B_{ij}\frac{z}{R}$, where $A_{ij}$ and $B_{ij}$ are dimensionless parameters, and z is the thickness variable. Assuming negligible stresses through the thickness (i.e., $\sigma_{zz}$), the stress components have the form $\sigma_{ij} = \frac{E}{1-\nu^2}[C_{ij} + D_{ij}\frac{z}{R}]$, where $C_{ij}$ and $D_{ij}$ are nondimensional coefficients depending on the Poisson's ratio. With these expressions for strain and stresses, the internal force resultants take the form $F_{ij} = \frac{Eh}{1-\nu^2}C_{ij}$ and the internal moment resultants take the form $M_{ij} = \frac{Eh}{1-\nu^2}D_{ij}$. As before, $C_{ij}$ and $D_{ij}$ are nondimensional coefficients depending on the Poisson's ratio, but not on the size of the deformed middle surface. Therefore, if the size is scaled and Poisson's ratio is held fixed, E, h, and the other quantities of the system such as spin rate may be scaled in such a way that the shape of the deformed middle surface is the same in the test as in the actual vehicle.

## 9.3 Model Diaphragm

The design of the model diaphragm was driven by two requirements: 1) accurate geometric scale, including thickness and details of the ribs; 2) and the modulus of elasticity sufficiently high to allow testing in the spin speed range of 1000-2000 rpm. Spin speeds of this magnitude usually give enough nutation cycles for accurate drop test results.

The decision was made early on in the program to develop an injection mold. The mold consists of male and female hemispherical surfaces which are moved into close proximity, separated by the desired diaphragm wall thickness of 0.0187 inches. Plastic pellets are placed in a hopper, heated to the melting point, and the fluid injected under high pressure. The material enters the hemispherical cavity at the pole, flows around the surface and exits at the rim of the equator. The excess material (flash) is later trimmed off. The desirable aspect of injection molding is that there is a wide rangle of plastics available. Therefore, at least potentially, diaphragms of virtually any desirable stiffness could be manufactured. Another important reason that an injection mold was chosen is that it can also be used for compression molding using rubber. In compression molding the raw rubber material is inserted between the two mold halves and they are squeezed together. This compresses the rubber and forces it to fill the mold cavity. The part is then removed and cured at high temperature. This vulcanizing process changes the internal structure of the material and increases the stiffness. The first diaphragms made used low density polyethylene in an injection process. It proved to be extremely difficult to produce a whole diaphragm using this process, although eventually about six accurate parts were made. Hundreds of parts were discarded because only part of the mold was filled. It was difficult to keep the two halves of the mold in the desired relative orientation as the molten plastic was injected due to hydraulic action shifting the mold and tight tolerances dictated by the thin (0.0187 inch) desired wall section. About three parts were made using a higher density polyethylene but these were even more difficult to obtain and were so stiff that the diaphragm could not be reversed (turned inside out) without breaking. There were no breakage problems with those made from the

low density material, and these were used for all of the drop tests. They have a modulus of elasticity of 40,000 psi, resulting in a model spin speed of 1200 rpm. After the injection molded parts were made, the compression molding process was used using rubber compounds specially blending for this project. Different proportions of styrene and natural rubber are blended to create materials of varying stiffness. Two such blends were used for this project, resulting in values for E of 20,800 and 44,800 psi. The respective spin speeds are 870 rpm and 1300 rpm. Higher stiffness rubber diaphragms for subsequent tests for the following reasons: 1) the compression molded rubber units were easier to manufacture in case more were needed; 2) for a given modulus of elasticity, the rubber diaphragm appeared to be deformed more readily than the polyethylene diaphragm without breaking; 3) since the full-scale diaphragm was made out of a rubber compound, it was assumed that the rubber model diaphragm would be more likely to match Poisson's ratio.

# 10 Phase IIb-DS1 Hydrazine Tank Drop Test Program

Phase IIb of the DS1 hydrazyne tank test program was also succesfully completed. A newly developed rubber diaphragm was used for all the tests. This was easier to stretch than the plastic version used in Phase IIa, allowing the desired fill level of 87.5 percent to be reached (with the plastic diaphragm, the maximum fill level was 85 percent). Models representing the pre- and post-burn state were tested at the nominal inertia ratio and for values approximately 10 percent higher and lower than the nominal. All results show very long time constants.

The parameters of the drop test model are as follows:

| | |
|---|---|
| Tank diameter | 4.75 inches I.D. |
| Liquid | Water, 87.5 percent fill level |
| Diaphragm Thickness | 0.019 inches |
| Diaphragm Young's modulus | 44,750 psi |
| Diaphragm material | blend of natural rubber and styrene |
| Nominal spin rate | 1300 rpm |

The 4.75 inch model tank defines the length scale to be 1/3.47, which then defines the diaphragm thickness to be 0.019 inches. The diaphragm stiffness scaling law $E/\rho R^2\omega^2$ discussed in the section describing Phase 1 defines the model spin rate of 1300 rpm.

The drop test model is composed of six parts: a 24 inch long, 6-inch diameter PVC tube; a fuel tank; two aluminum end caps (the left cap is considered the forward end, and the right end is considered the aft end, closest to solid motor, and carries the model telemetry electronics); a 22 pound solid steel weight fastened to the tube (this represents the solid motor); a lead ring fastened to the outer surface of the tube to alter the inertia ratio. The pre-burn and post-burn models differ only in tank location. The tank center is 2.8 inches from the left end of the tube for pre-burn, and 11.8 inches for post-burn. In each case, the distance between the tank center and the cm of the model (cm offset) is correctly scaled.

# 11 Test results

The first test done was a tare test (no liquid in tank) to verify the lack of parasitic energy dissipation in the dry model. The model constant was an extremely long 45 seconds. The full scale time constant was computed by inertia scaling using the standard scaling law $\rho R^5\omega\tau/J$, where $\rho$ is the liquid density, R is the tank radius, $\omega$ is the spin speed, $\tau$ is the time constant, and J is the spin inertia. The model spin inertia varies slightly when

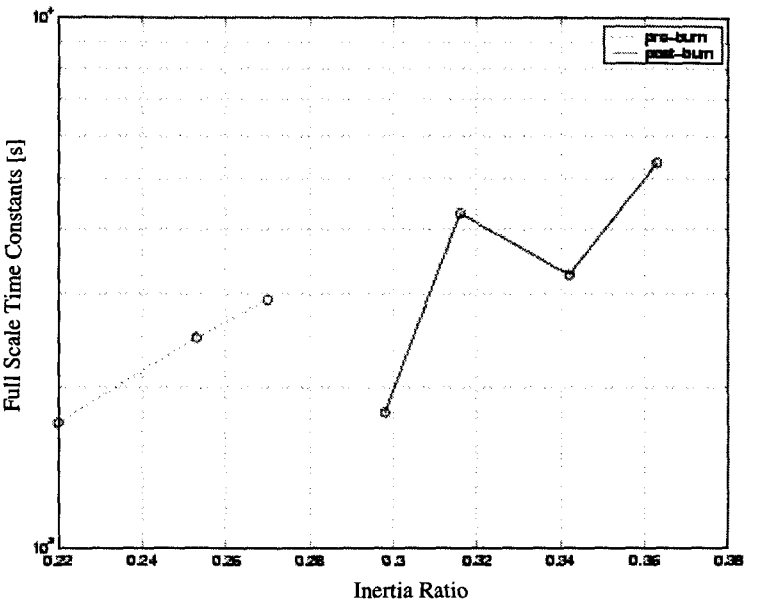


Figure 12: Full scale pre- and post-burn time constants vs. inertia ratio for the hydrazine tank.

inertia ratio weights are added but the scaling is approximately $\tau_{fullscale} = 98\tau_{model}$ for the pre-burn case, and $\tau_{fullscale} = 59\tau_{model}$ for the post-burn case. The actual model spin inertias are used to compute the full-scale time constant.

Figure 12 shows a plot of the time constants for the test results in the pre-burn and post-burn cases. For this test program, a high confidence level exists for model time constants shorter that about 5 seconds. For values longer than 5 seconds (all test results), there is uncertainty in the results, which explains the scatter in the data. When dealing with very long time constants, as in this test program, it would also be more meaningful to speak in terms of inverse time constant, since that reflects the energy dissipation rate more accurately. Finally, Figure 13 depicts the sensitivity of the nutation time constant to the liquid fill fraction.

# 12 Flight Test Results

Figure 14 shows the pitch acceleration, thrust acceleration, NTC tank pressure, and filtered rate gyro vs. time during Star-38 ignition and burnout, respectively (courtesy of James Corbo, Boeing Astronautics). These plots confirm the reuslts of the analysis and testing in that the nutation barely developed in these phases of the DS1 flight.

# 13 Conclusions

The conclusions of this paper are as follows:

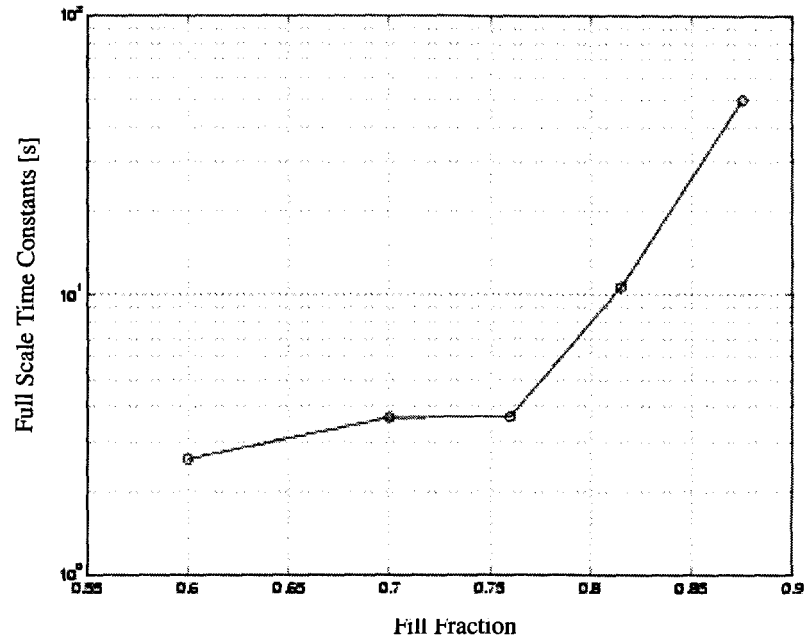


Figure 13: Full scale time constants vs. fill fraction for the hydrazine tank.

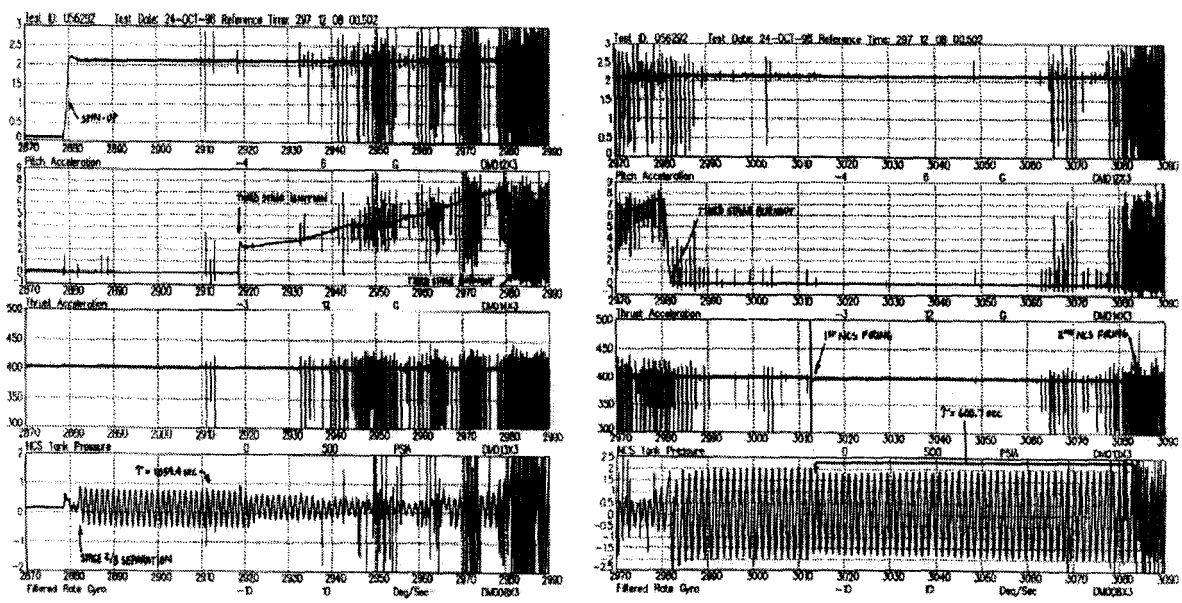

Figure 14: Pitch acceleration, thrust acceleration, NTC tank pressure, and filtered rate gyro vs. time during Star-38 ignition (right) and burn-out (left). Courtesy of James Corbo, Boeing Astronautics.

- Several modelling issues are described, particularly concerning the effect of the membrane in the hydrazine tank. An energy sink analysis gives an initial estimate for the nutation time constant of $\tau = 25354$ seconds at ignition, and of $\tau = 14660$ seconds at burn-out. We observe that, assuming a perfect mass balance, liquid slosh is probably not an issue in this type of diaphragm tank configuration. The only uncertain dynamic response was in terms of liquid resonances (inertial wave modes) which might have been excited inside the Xenon and the Hydrazine tanks.

- Three different approaches to solving the problem of liquid slosh in spinning tanks have been reviewed. First, pendulum models are described to capture the first slosh modes, but no inertial modes. Second, a linearized coupled rigid-spacecraft/fluid-dynamics approach is described to capture both the slosh and inertial modes. Third, a fully nonlinear coupled rigid-spacecraft/fluid-dynamics approach is described which captures all the modes via a computational fluid dynamics approach. The third model, although very computationally intensive, is recommended for additional study and computations for nutation time constant determination.

- In order to simulate the nonlinear behavior of the spacecraft containing the liquid (Hydrazine), the dynamics of a rigid body coupled through a universal joint to a pendulum mass representing the liquid slosh has been analyzed. Despite the uncertainty in diaphragm viscoelastic properties, the results of the analysis show that the nutation time constant is $\tau = 1590$ seconds at ignition, and $\tau = 1990$ seconds at burn-out. The fact that these two numbers are not very different can be intuitively explained because of the very large tank fill factor, which approximates the behavior of this tank to that of a fully filled spherical tank.

- Dimensional analysis on a model of the tank with diaphragm identifies the relevant parameters which influence the dynamics of an on-axis spinning tank with a flexible diaphragm . Through dimensional analysis, we obtain a new estimate of the nutation time constant including the effect of the stiffness and damping of diaphragm. We also identify two new dimensional groups, the elastic Bond number which rules the elasticity of the diaphragm, and the elastic Reynolds number, which rules the damping in the diaphragm. These effects, as well the effect of fill factor, fluid Reynolds, Bond, and Froude numbers, and tank location with respect to spacecraft center of mass, have to be determined experimentally with air bearing tests, spin drop tests, or energy dissipation tests. General considerations based also on Bond number estimates including also the effect of membrane tension point out the different regimes of liquid motion which would require different modeling approaches should a more sophisticated analysis need to be done.

- Spin drop tests were done by Dr. Jon Harrison of Applied Dynamics Laboratories (Roseburg, OR). These tests also confirm a nutation time constant in excess of 1000 seconds, both in the case of tests done for tha Xenon tank only and in the case of tests done for the Hydrazine tank only.

- Flight data reports a small number of Nutation Control System firings, and Nutation Time Constants of 1055 seconds (pre-burn) and 605 seconds (post-burn), confirming the analysis and test results.

**Acknowledgments**: The research described in this paper was carried out at the Jet Propulsion Laboratory, California Institute of Technology, under a contract with the National Aeronautics and Space Administration. The author is grateful to Dr. Sam Sirlin, Dr. Dankai Liu, and Mr. Mike Davis of JPL for financial and intellectual support, to Dr. Jon Harrison of Applied Dynamics Laboratories, Inc. for conducting the drop tests, to Mr. Mike Marcucci of JPL for providing Figure 2, to Dr. Carl Hubert of Hubert Astronautics, Inc. for providing useful information on the nutation synchronous mode, and to Mr. James Corbo of Boeing Astronautics for providing the flight test data.

# 14 REFERENCES

[1] Abramson, H.N.: *The Dynamic Behavior of Liquids in Moving Containers*,NASA SP-106, 1966.

[2] Alfriend, K.T.: *Partially Filled Viscous Ring Nutation Damper*, Journal of Spacecraft and Rockets, vol. 11, no. 7, 1974, pp. 456-462.

[3] Cartwright, Massingill, and Trueblood: *Circular Constraint Nutation Damper*, AIAA Journal, vol. 1, no. 6, 1963, pp. 1375-1380.

[4] Dodge, F.: *Propellant Dynamics And PMD Design For The Near Earth Asteroid Rendezvous (NEAR) Spacecraft*, SWRI Project 04-6297, Southwest Research Institute, April 1994.

[5] Dodge, F.T. and Kana, D.D.: *Dynamics Of Liquid Sloshing In Upright And Inverted Bladdered Tanks.* 1985

[6] Dodge, F.T., : *Slosh Investigation*, Final Report to RCA, SWRI Project 06-1378-101, April 20, 1987.

[7] El-Raheb, M., and Wagner, P.: *Vibration of a Liquid With A Free Surface In A Spinning Spherical Tank*, Journal of Sound and Vibration, Vol. 76, Part 1, 1981, pp. 83-93.

[8] Greenspan, H.P.:*The Theory of Rotating Fluids*,Cambridge University Press, 1969.

[9] Harrison, J.: *Analysis of spacecraft nutation dynamics using the drop test method*, Space Communications and Broadcasting, vol. 5, 1987, pp. 265-280.

[10] Hubert, C.: *Assessment of MSP Lander Propellant Dynamics During Spinning Operations*, Hubert Astronautics Report, 30 January 1997.

[11] Hubert, C.: *Deep Impact Nutation Assessment*, Hubert Astronautics Report, 3 July 2002.

[12] Kana, D.D., : *Validated Spherical pendulum Model for Rotary Liquid Slosh*, Journal of Spacecraft and Rockets, vol.26, no.3, pp.188-195.

[13] Kana and Dodge: *Preliminary Study of Liquid Slosh in the Tracking and Data Relay Satellite Hydrazine Tanks*, Final Report of Project 02-5887, Southwest Research Institute, San Antonio, TX, December 7, 1979.

[14] Kreis, A., Kurz, A., Klein, M., Deloo, Ph.: *Static and Dynamic Modeling of Diaphragm Tanks*, Proc. Conference on Spacecraft Structures, Materials, and Mechanical Testing, Noordwijk, The Netherlands, 27-29 March, 1996.

[15] McIntyre, J. E. and Tanner, T. M.: *Fuel Slosh in a Spinning On-Axis Propellant Tank: An Eigenmode Approach*, Space Communication and Broadcasting, no. 5, 1987, pp. 229-251.

[16] Mingori L. and Harrison J.: *Circularly Constrained Particle Motion in Spinning and Coning Bodies*, AIAA Journal, vol. 12, no. 11, 1974, pp.-1553-1558.

[17] Marce, J. et al.: *Energy Dissipation In Exosat Tanks - Test Results*, CNES Technical Note, CNES-NT-99, March 1981.

[18] Quadrelli, M.: *Final Report of Deep Space 1 Nutation Time Constant Analysis and Testing*, Internal JPL Engineering Memorandum EM-3455-98-01, February 18, 1998.

[19] Ross, R.G., and Womack, J.R.:*Slosh Testing of a Prototype Electric Propulsion Mercury Propellant Tank with Positive Expulsion Diaphragm*, AIAA paper 73-1120, presented at the 10th Electric Propulsion Conference, Lake Tahoe, NV, October 31-Nov. 2, 1973.

[20] Sirlin, S.W.: *Mars Pathfinder Launch Vehicle Nutation Analysis*, IOM-3456-96-032, JPL, 19 July 1996.

[21] Stofan, A. and Pavli, A.: *Experimental Damping Of Liquid Oscillations In A Spherical Tank By Positive Expulsion Bags And Diaphragms*, NASA TN-D-1311, July 1962.

[22] Stofan, A.J. and Sumner, I.E.: *Experimental Investigation Of The Slosh-Damping Effectiveness Of Positive Expulsion Bags And Diaphragms In Spherical Tanks*, NASA TN-D-1712, June 1963.

[23] Wood, J., *Mars '98 Lander Nutation Time Constant Estimate Issues*, VSG-ML-M-0897-003R1, 18 August 1997.

[24] Zedd, M.F., and Dodge, F.T, :*Energy dissipation of liquids in nutating spherical tanks measured by a forced motion spin table.* AIAA paper 84-1842, 1984.